Published in "European Journal of Mineralogy 23(5): 731-743, 2011"
which should be cited to refer to this work.

Severe structural damage in Cr- and V-rich clinozoisite: relics of an epidote-group mineral with $Ca_2Al_2Cr^{3+}Si_3O_{12}(OH)$ composition?

MARIKO NAGASHIMA[1,2,*], THOMAS ARMBRUSTER[1], MARCO HERWEGH[3], THOMAS PETTKE[3], SEPPO LAHTI[4] and BERNARD GROBÉTY[5]

[1] Mineralogical Crystallography, Institute of Geological Sciences, University of Bern, Freiestrasse 3, 3012 Bern, Switzerland
[2] Graduate School of Science and Engineering, Yamaguchi University, 1677-1 Yoshida, Yamaguchi 753-8512, Japan
*Corresponding author, e-mail: nagashim@yamaguchi-u.ac.jp
[3] Institute of Geological Sciences, University of Bern, Baltzerstrasse 1+3, 3012 Bern, Switzerland
[4] Geological Survey of Finland, P.O. Box 96, 02151 Espoo, Finland
[5] Institut de Minéralogie et Pétrographie, Université de Fribourg, 1700 Fribourg, Switzerland

Abstract: Cr-rich clinozoisite with up to 0.89 Cr^{3+} apfu and additional 0.23 V^{3+} apfu originating from the Outokumpu copper mine, Finland, was studied by electron microprobe analyses, laser ablation inductively coupled-plasma mass spectrometry, single-crystal X-ray structure refinement of natural crystals and after step-wise annealing to a maximum temperature of 750°C, by HRTEM and electron backscattered diffraction. Although Cr-rich clinozoisite appears optically of gemmy quality with sharp extinction behavior under crossed polarizers, its X-ray and electron-diffraction behavior is very poor and resembles that of almost amorphous materials as known for strong metamictization. Albeit the sample does not contain significant U or Th as potential source of radiation and destruction of lattice periodicity. Cr- and V-free clinozoisite, intergrown with Cr- and V-rich clinozoisite, displays good diffraction behavior. Cr- and V-rich clinozoisite of poor diffraction quality has larger unit-cell volume than expected for its composition. The volume decreases with increasing annealing but does not reach the range expected for the analyzed composition. Heating cycles slightly improve crystallinity but the diffraction quality remains unsatisfactory. Site occupancy refinements of single-crystal X-ray data collected for natural crystals after heat treatment could not reproduce the (Cr + V) concentration previously determined by analytical methods. We speculate that probably on the retrograde path nano-particles of a Cr-(and V-) rich amorphous phase were exsolved destroying the periodicity of the residual clinozoisite. Annealing led to substantial structural cure but the original (Cr + V) content could not be reabsorbed.

Key-words: clinozoisite, epidote, chromium, vanadium, Outokumpu, amorphous, metamict, ''tawmawite''.

1. Introduction

Monoclinic epidote-group minerals with the structural formula A1A2M1M2M3Si_3O_{12}(OH) belong to the soro/neso-silicate class. Their structure is based on a chain of edge-sharing M2 octahedra and a central chain of M1 octahedra with M3 octahedra attached on alternate sides along its length. Chains of octahedra run parallel to the **b**-axis, linked by SiO_4 and Si_2O_7 groups (Ito *et al*., 1954; Dollase, 1968). This structural arrangement gives rise to two types of highly coordinated sites: 9-coordinated A1 and 10-coordinated A2 are mainly occupied by Ca. Trivalent cations, such as Al, Fe^{3+}, Mn^{3+} and Cr^{3+}, distribute between the octahedral M1 and M3 sites. The smallest $M2O_6$ octahedron is generally occupied by Al only. The key cation-sites M3 and A1 determine the root name, and for the dominant cation on A2 (other than Ca) the suffix designation is used. This paper follows the recommended nomenclature for epidote-group minerals summarized by Armbruster *et al*. (2006).

Epidote-group minerals containing Cr^{3+} are not common, but they have been reported from a number of localities worldwide (*e.g*., Eskola, 1933; Grapes, 1981; Ashley & Martyn, 1987; Treloar, 1987a, b; Treloar & Charnley, 1987; Sánchez-Vizcaíno *et al*., 1995; Devaraju *et al*., 1999; Nagashima *et al*., 2006, 2007, Uher *et al*., 2008, Bačík & Uher, 2010). The term ''tawmawite'' was proposed for the Cr^{3+}-analogue of epidote (Bleeck, 1907). However, ''tawmawite'' from former ''Burma'' (nowadays Myanmar) does not show epidote-group stoichiometry and may reflect a mixture of various Cr-bearing minerals. The highest Cr_2O_3 content of *ca*. 15 wt% for an epidote-group mineral was reported by Treloar (1987a, b) corresponding to almost 1 Cr atom per formula unit (apfu). However, for

revival of ''tawmawite'' as a valid mineral name for a species of the epidote-group it has to be shown that Cr is the dominant cation at one of the three octahedral sites (M1–M3). Up to now, there is no structural study of an epidote-group mineral with more than 0.5 Cr apfu at any M site. Thus, ''tawmawite'' is not considered a valid species name (Armbruster *et al*., 2006).

A crystal structure of Cr^{3+}-bearing epidote has been reported by Nagashima *et al*. (2007). The site preference of Cr^{3+} is M3 > M1 >> M2 although the results of a polarized absorption spectroscopic study by Burns & Strens (1967) have been interpreted to show preference of Cr^{3+} for M1. In an experimental study of the binary $Ca_2Al_3Si_3O_{12}(OH)$-$Ca_2Al_2Cr^{3+}Si_3O_{12}(OH)$ series (Nagashima *et al*., 2009) the maximum Cr content in clinozoisite was 0.5 apfu. The intracrystalline partitioning coefficient, $K_D = (Cr^{3+}/Al)^{M1}/(Cr^{3+}/Al)^{M3}$, ranged between 0.57 and 0.73 indicating preference of Cr^{3+} for M3 > M1.

Subject of this study is the crystal chemistry of Cr-rich clinozoisite, leading to the decisive question whether a Cr-analogue $Ca_2Al_2CrSi_3O_{12}(OH)$ of epidote may exist.

2. Experimental methods

2.1. Specimens

2.1.1. Cr- and V-rich clinozoisite from Outokumpu copper mine, Finland

Chromium-rich clinozoisite crystals from Outokumpu copper mine, Finland, were first described by Eskola (1933) and later studied by von Knorring *et al*. (1986) and Treloar (1987a, b). According to Treloar (1987a) the Cr content in clinozoisite from the Outokumpu mine reaches 15.4 wt% Cr_2O_3. The crystals we studied were received from some Finnish mineral collectors and from the Mineral Cabinet of the Finnish Museum of Natural History, University of Helsinki. The museum specimens are of historic significance, because mining operations in the Outokumpu mine ended already in 1988. According to the sample labels, they were collected by Eskola for his studies published in 1933.

The Outokumpu Cu-Zn ± Co ore hosts carbonate-skarn rock, quartzite and serpentinite. The deposit is an ophiolitic volcanogenic massive sulfide ore formed by multi-stage deformation processes during the Paleoproterozoic Svecokarelian orogeny 1.75-1.9 Ga ago (Koistinen, 1981; Treloar *et al*., 1981). According to Treloar *et al*. (1981) the Cr-bearing minerals reflect metamorphic conditions of 3.5 ± 1 kbar and 600 ± 50 °C.

The skarn rocks of the Outokumpu area are enriched in chromium and vanadium. The Outokumpu mine is, for example, the type locality for eskolaite (Cr_2O_3) and karelianite (V_2O_3). The Cr-rich clinozoisite that also may contain considerable vanadium concentrations locally occurs as accessory in ore-bearing quartzite and especially in ore-bearing skarn rocks composed mainly of chromian diopside, chromian tremolite and uvarovite. The chromian and vanadian clinozoisite crystals are prismatic, 1–10 millimeters long and they may contain simple crystal faces like {100}, {001}, {011}, {101} and {110}.

The crystal fragments chosen for this study were some millimeters in diameter. They were often strongly zoned and contained also additional phases as inclusions (see below). Standard thin sections and also thick sections were prepared from the specimens, which were used for electron microprobe analyses (see experimental section). In thin sections, independent of the Cr-content, clinozoisite showed sharp extinction behavior under crossed polarizers. In polarized light, Cr-rich crystals displayed characteristic pleochroism from yellow-green to blue-green. In thick sections (*ca*. 300 μm), used for single-crystal harvesting for structural study, fragments of Cr-rich clinozoisite appeared in unpolarized light emerald-colored with gemmy transparence and high optical quality without visible inclusions, but were commonly fractured by scattered cracks.

Chemical analyses indicate that our specimens can be divided into three types: (1) Cr- and V-rich, (2) Cr- and V-bearing, and (3) Cr- and V-free clinozoisite varieties. For details of this classification see the Result section. In several crystals Cr-bearing clinozoisite exhibited fine oscillatory zoning by layers with strongly variable Cr/Al content. Such ''crystals'' were not considered.

According to electron-microprobe analyses the associated phases, enclosed within the macroscopic Cr-bearing clinozoisite crystals, are chromian tremolite, chromian diopside, uvarovite, pyrite, pyrrhotite, chalcopyrite, a zinc sulfide phase, eskolaite, quartz, albite, and an unidentified sheet-silicate-like Cr-rich mineral also observed by Treloar (1987a), which he described as alteration product of Cr-rich clinozoisite: ''complex hydrated Cr-Mg-A1-Fe-Ca-bearing silicate, the composition of which approaches a hydrogarnet type stoichiometry. The degree of hydration varies from slight to extreme.''

A typical mineral association is shown in Fig. 1. The core of the crystal mainly consists of Cr- and V-bearing clinozoisite, which is pale green in color. The unidentified sheet-silicate-like Cr-rich mineral (mentioned before) occurs as greenish-brown ribbons of variable thickness and it is commonly associated with Cr- and V-bearing clinozoisite (Fig. 1a). Appearance of this mineral indicates that it forms layer-like inclusions (exsolutions), which were cut to bands depending on the inclination angle during thin-section preparation. The outer zones of the investigated Cr-bearing clinozoisite crystals formed under low fO_2 condition as indicated by pyrite (commonly <100 μm) and chalcopyrite (<50 μm) occurring as inclusions in Cr- and V-free clinozoisite, associated with albite. Cr- and V-rich clinozoisite showing dark brownish green color forms the inner rim of the ''crystal'' but an additional thin Cr- and V-free clinozoisite phase commonly crystallized at the last stage on the surface. Although Cr-rich allanite (up to 5.7 wt% Cr_2O_3) in mica schist from Outokumpu was reported by Treloar (1987b) and Treloar & Charnley (1987), rare earth element concentrations were below the detection

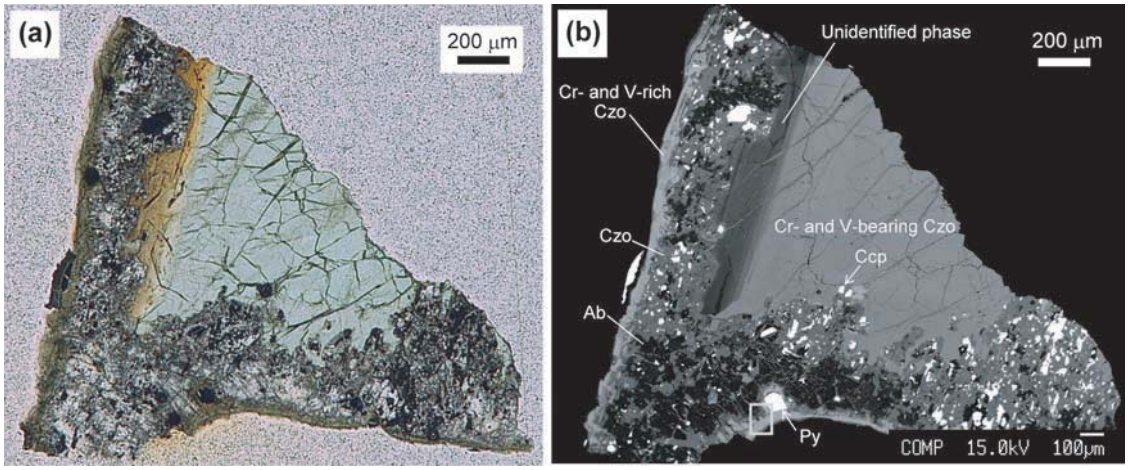

Fig. 1. Photomicrograph (a) and back-scattered electron image (b) of clinozoisite (Czo) and associated phases, pyrite (Py), chalcopyrite (Ccp), albite (Ab), and an unidentified sheet-silicate-like Cr-rich mineral. Box at the bottom in BSE image indicates an area analyzed by EBSD (see Fig. 5).

limit in specimens analyzed in this study. Furthermore, the source rock of Cr-bearing clinozoisite in this study was quartzite in contrast to mica schist in which allanite was analyzed.

2.1.2. Cr-bearing epidote from Iratsu, central Shikoku, Japan

A Cr-bearing epidote from Sambagawa metamorphic rocks in central Shikoku, Japan (Nagashima *et al*., 2006, 2007) was re-investigated. These Cr-rich epidote crystals are dark yellow to brown. Microscopically, they are subhedral and are pleochroic from yellowish orange to pale yellow-colorless.

2.2. Chemical analysis

2.2.1. Electron microprobe analysis

The chemical composition of Outokumpu clinozoisite was determined using a JEOL JXA-8200 electron probe microanalyzer (EPMA/WDS) at the University of Bern. The abundances of Si, Ti, Al, Cr, V, Fe, Mn, Mg, Ca, Sr, Ba, Na, K, Zn, P and F were measured using an accelerating voltage of 15 kV and a beam current of 20 nA, with a beam diameter of 1 μm. The following standards were used: natural wollastonite (Si, Ca), synthetic ilmenite (Ti, Fe), synthetic spinel (Al, Mg), synthetic eskolaite (Cr), synthetic shcherbinaite (V), synthetic tephroite (Mn), natural strontianite (Sr), natural barite (Ba), natural albite (Na), natural orthoclase (K), synthetic gahnite (Zn), synthetic $CePO_4$ (P), and synthetic phlogopite (F). The PRZ method (modified ZAF) with $\phi(\rho Z)$ integration for the atomic number correction (Packwood & Brown, 1981; Bastin *et al*., 1984, 1986) was used for data correction. Some elements were not detected or negligible. The peak positions of Cr$K\alpha$ and V$K\beta$ measured with the LIF analyzer crystal are very close, and the Cr$K\alpha$ peak slightly overlapped with V$K\beta$. To obtain proper intensity of Cr$K\alpha$, the intensity correction was applied for each analytical point. Experimental details of chemical analyses for Cr-bearing epidote from Iratsu, Japan, have been summarized by Nagashima *et al*. (2006).

2.2.2. Laser ablation inductively coupled-plasma mass spectrometry (LA-ICP-MS)

The chemical composition of (Cr + V)-rich clinozoisite was also confirmed by laser ablation, inductively coupled-plasma mass spectroscopy (LA-ICP-MS). The instrument consists of a pulsed 193 nm ArF Excimer laser (Lambda Physik, Germany) with an energy-homogenized Geolas Pro optical system (Microlas, Germany), coupled with an ELAN DRC–e ICP quadrupole mass spectrometer (Perkin Elmer, Canada) operated in standard mode. A spot size between 60 and 90 μm was used and the counting time was >50 s for the background and 50 s for sample analysis. The instrument was calibrated against NIST SRM 610 glass.

2.3. Structural analysis of Cr-rich and Cr–bearing clinozoisite and epidote

Diffraction data of five crystals, separated from previously analyzed (EPMA) thick-sections, were collected at room temperature (23 °C) with graphite-monochromated Mo$K\alpha$ X-radiation ($\lambda = 0.71069$ Å) using different types of single-crystals diffractometers, either equipped with a point detector (Enraf Nonius CAD4) or with a CCD-based area detector (Table 1). All crystals except for 2E and the Iratsu epidote were heated at different temperatures in air and subsequently remeasured and reheated. As an example, crystal 1A was heated at 500, 600, 700 and 750 °C for 20 h at each temperature. Annealing was done to enhance sample crystallinity.

For all samples, structural refinements were performed using SHELXL-97 (Sheldrick, 2008). Scattering factors for neutral atoms were employed. In all refinements on

Table 1. Crystallographic data and experimental details for the single-crystal X-ray diffraction analysis.

	Outokumpu, Finland											
	1A					1C			1E		2E	Iratsu, Japan
Heating temperature (°C)	No treatment	500	600	700	750	No treatment	600	750	No treatment	700	No treatment	No treatment
Duration (h)		20	20	20	20		48	48		24		
Row color of crystal	Green	Grayish green	Grayish green	Yellowish brown	Yellowish brown	Green	Yellowish brown	Black	Green	Grayish green	Green	Yellow
Space group	$P2_1/m$					$P2_1/m$			$P2_1/m$		$P2_1/m$	$P2_1/m$
Crystal size (mm)	0.20 × 0.18 × 0.10					0.13 × 0.09 × 0.06			0.25 × 0.20 × 0.10		0.20 × 0.18 × 0.50	0.185 × 0.15 × 0.05
Cell parameters a (Å)	8.977(6)	8.923(5)	8.925(5)	8.899(3)	8.883(3)	8.972(1)	8.9344(8)	8.926(2)	8.906(1)	8.8887(2)	8.906(2)	8.8914(1)
b (Å)	5.689(4)	5.654(3)	5.647(3)	5.624(2)	5.616(2)	5.6934(7)	5.6582(7)	5.655(1)	5.6241(5)	5.6114(5)	5.6257(9)	5.6194(1)
c (Å)	10.261(6)	10.226(6)	10.212(6)	10.197(4)	10.191(4)	10.264(1)	10.2372(9)	10.255(2)	10.162(2)	10.152(2)	10.165(2)	10.1611(1)
β (°)	115.525(7)	115.598(6)	115.572(6)	115.575(4)	115.597(4)	115.387(6)	115.455(5)	115.540(4)	115.21(1)	115.23(2)	115.21(2)	115.175(1)
V (Å^3)	474.2(2)	465.3(2)	464.7(2)	460.4(1)	458.5(1)	473.7(2)	467.3(1)	467.0(1)	460.5(2)	458.0(4)	460.8(5)	459.47(2)
D calc (g/cm^3)	3.145	3.218	3.233	3.256	3.268	3.245	3.288	3.290	3.322	3.336	3.319	3.378
Diffractometer	Siemens Smart CCD 1K					Bruker APEX CCD			CAD4 Enraf-Nonius			Bruker APEX CCD
Scan type	ω scan					ϕ and ω scans (Bruker,1999)			ω scan (Enraf-Nonius, 1983)			ϕ and ω scans (Bruker, 1999)
Absorption correction	Semi-empirical[a]					SADABS (Sheldrick, 1996)			ψ scan (Enraf-Nonius, 1983)			SADABS (Sheldrick, 1996)
θ_{min}(°)	2.2	2.5	2.5	2.5	2.5	2.2	2.2	2.2	2.2	2.2	2.2	2.2
θ_{max}(°)	27.4	27.5	27.2	27.2	27.3	27.4	27.5	24.3	40.0	29.9	27.0	35.1
μ (mm^{-1})	2.42	2.46	2.47	2.49	2.50	3.59	3.634	3.64	11.21	11.27	2.49	6.205
Collected reflections	3044	2995	2872	2844	2829	2923	2852	3083	5118	1824	1165	11575
Unique reflections	1107	1076	1061	1046	1060	1183	1167	842	3048	1457	1105	2186
R_{int} (%)	6.19	5.15	3.92	3.20	3.28	5.39	3.88	5.80	1.47	1.12	1.78	1.95
R_{sigma} (%)	5.62	5.56	4.34	3.07	3.02	10.58	6.67	5.86	3.05	1.63	4.37	1.38
Miller index limits	$-11\le h\le 11$, $-7\le k\le 5$, $-13\le l\le 12$	$-10\le h\le 11$, $-6\le k\le 7$, $-10\le l\le 13$	$-10\le h\le 11$, $-7\le k\le 7$, $-12\le l\le 12$	$-10\le h\le 11$, $-6\le k\le 6$, $-12\le l\le 12$	$-10\le h\le 11$, $-6\le k\le 7$, $-12\le l\le 11$	$-11\le h\le 11$, $-6\le k\le 7$, $-9\le l\le 13$	$-11\le h\le 9$, $-3\le k\le 7$, $-12\le l\le 13$	$-10\le h\le 10$, $-6\le k\le 6$, $-11\le l\le 11$	$-16\le h\le 14$, $-5\le k\le 10$, $-14\le l\le 18$	$-12\le h\le 11$, $0\le k\le 7$, $-2\le l\le 14$	$-11\le h\le 10$, $0\le k\le 7$, $0\le l\le 12$	$-14\le h\le 14$, $-8\le k\le 9$, $-16\le l\le 16$
R_1 (%)	7.60	5.17	4.29	3.38	3.40	6.31	5.27	5.03	2.61	1.92	2.49	2.02
wR_2 (%)	18.12	11.63	9.39	7.44	8.10	18.74	14.75	13.93	7.62	5.45	7.13	5.74
Weighting scheme	$w = 1/[\sigma^2(F_o^2) + (0.0556P)^2 + 6.15P]$	$w = 1/[\sigma^2(F_o^2) + (0.0376P)^2 + 2.44P]$	$w = 1/[\sigma^2(F_o^2) + (0.0295P)^2 + 1.95P]$	$w = 1/[\sigma^2(F_o^2) + (0.0253P)^2 + 1.11P]$	$w = 1/[\sigma^2(F_o^2) + (0.0355P)^2 + 0.80P]$	$w = 1/[\sigma^2(F_o^2) + (0.0690P)^2 + 4.70P]$	$w = 1/[\sigma^2(F_o^2) + (0.0635P)^2 + 2.53P]$	$w = 1/[\sigma^2(F_o^2) + (0.0411P)^2 + 7.76P]$	$w = 1/[\sigma^2(F_o^2) + (0.0365P)^2 + 0.37P]$	$w = 1/[\sigma^2(F_o^2) + (0.0256P)^2 + 0.56P]$	$w = 1/[\sigma^2(F_o^2) + (0.0375P)^2 + 0.58P]$	$w = 1/[\sigma^2(F_o^2) + (0.0251P)^2 + 0.40P]$
$\Delta\rho_{max}$ (e Å^{-3})	2.328	1.790	1.541	1.269	1.282	2.103	2.059	1.829	1.854	0.928	1.049	0.811
$\Delta\rho_{min}$ (e Å^{-3})	–0.682	–0.621	–0.506	–0.512	–0.453	–0.853	–0.892	–0.679	–1.126	–0.390	–0.474	–0.634

Notes: Intensity data were measured using graphite-monochromatized Mo$K\alpha$ radiation (λ = 0.71069 Å). Structural refinement was performed using SHELXL-97 (Sheldrick, 2008). The function of the weighting scheme is $\omega = 1/[\sigma^2(Fo^2) + (a\cdot P)^2 + b\cdot P]$, where $P = [\mathrm{Max}(Fo^2, 0) + 2Fc^2]/3$, and the parameters a and b are chosen to minimize the differences in the variances for reflections in different ranges of intensity and diffraction angle. Densities were calculated based on the refined site occupancies shown in Table 7.

[a]A semi-empirical absorption-correction based upon the intensities of equivalent reflections was done by modeling the crystal as an ellipsoid (program XPREP, part of the Bruker (1999) package).

Outokumpu samples M2 seemed to be fully occupied by Al. Thus Cr and Al were allowed to vary at M1 and M3. Due to similarity of X-ray scattering factors additional V was treated as Cr.

The following procedures were applied to refine occupancies for the Iratsu sample: (1) A2 occupancy was fixed at Ca0.92 Sr0.08 as determined by EPMA. (2) Based on the results of Mössbauer spectroscopy (Nagashima *et al*., 2007), the oxidation state of Fe was ferric and all Fe was fixed at M3 (0.51 apfu). Site occupancies of M sites were refined with Al and Cr.

Positions of the hydrogen atoms of the hydroxyl groups were derived from difference-Fourier syntheses. Subsequently, hydrogen positions were refined at a fixed value of $U_{iso} = 0.05$ Å^2. The hydrogen positions were refined with a bond distance constraint of O–H = 0.98 Å (Franks, 1973).

2.4. HRTEM analysis

A powder sample of specimen 1A from Outokumpu, Finland, was analyzed with a Philips CM20 transmission electron microscope operated at 200 eV (point resolution of 0.27 nm) equipped with a twin objective lens (theoretical resolution 0.27 nm), a TV-Camera GATAN 622 with Image Intensifier and energy-dispersive X-ray (EDX) spectrometer. The Cr, V and Al contents of the sample were confirmed by EDX.

2.5. Electron backscattered diffraction (EBSD)

The EBSD analysis was carried out using only the specimens from Outokumpu, Finland. For this purpose the polished thin sections were subjected to an additional chemo-mechanical lapping on a polyurethane disk with colloidal silica during 5.5 h in order to remove preparation-induced defect structures in the uppermost nanometers.

The EBSD investigations were carried out under low vacuum conditions (10 Pa) using a Zeiss Evo 50 SEM in combination with an EDS Sapphire light element detector from EDAX-Ametek and a Digiview II EBSD camera as well as the OIM (5.31) acquisition and analysis software from TSL-Ametek. For the EBSD-mappings, an acceleration voltage of 20 kV, a beam current of 20 nA, a step size of 0.3 μm and a frame rate of 20 frames/s were chosen. Simultaneous with the acquisition of the electron diffraction pattern, the Si, Cr and Al concentrations were measured with the EDS detector. After analysis, data were processed using the OIM (5.31) analysis software for visualization of the image quality maps and the element distribution images.

In addition to the mapping approach, individual electron diffraction patterns were acquired at constant time intervals at specific spots on the Cr-rich clinozoisites to discriminate the degree of diffraction between the different microstructural domains.

3. Results

3.1. Chemical compositions

3.1.1. Cr-rich and Cr-bearing clinozoisite and epidote

The chemical compositions of the studied Cr-rich clinozoisite-subgroup crystals studied by X-ray diffraction are given in Table 2 where the total number of cations, except H^+, was normalized to 8. Figure 1b shows the back-scattered electron image of clinozoisite and associated phases from Outokumpu, Finland (116_2 crystal). Cr- and V-rich clinozoisite was mainly found at the rim of this grain adjacent to Cr- and V-free clinozoisite. The core of this crystal is composed of Cr- and V-bearing clinozoisite.

In a group with the highest Cr_2O_3 content we collected 13 analyses for Outokumpu clinozoisite with 10–14 wt% Cr_2O_3 and additional 2–8 wt% V_2O_3. Based on 159 analytical points measured on the same material, the mean Cr_2O_3 and V_2O_3 concentrations in Cr- and V-bearing clinozoisite, mainly constituting the core of the crystal, were 7.3 ± 1.1 and 2.4 ± 1.0 wt%, respectively. The range within this dominant group covered compositions with 5–10 wt% Cr_2O_3 and 1–6 wt% V_2O_3. Interestingly, there is a compositional gap in our analytical data: except ''(Cr + V)-free'' clinozoisite with less than 0.1 wt% Cr_2O_3 and V_2O_3 (10 points analyzed), there are no compositions with less than 5 wt% Cr_2O_3 (Fig. 2). If not explicitly specified the Cr_2O_3-high and Cr_2O_3-bearing groups will not be distinguished in the following text (named Cr-rich) as both types of clinozoisite show corresponding diffraction properties. The specimens from Outokumpu are poor in Fe_2O_3 (*e.g.,* ~0.4 wt% of 1A and 1E). The Cr content of Cr-rich clinozoisite (5.7–15.4 wt% Cr_2O_3) from the same locality studied by Treloar (1987a, b) was similar to that in this study. On the other hand, their samples were poor in V_2O_3 (max. 2.3 wt%) compared to our samples.

To confirm the accuracy of obtained Cr_2O_3 and V_2O_3 contents in Finnish samples by microprobe analysis, 13 points on three different crystals (2A, 2C and 2E) were also analyzed by LA-ICP-MS. The Cr_2O_3 and V_2O_3 contents obtained by EPMA and LA-ICP-MS were closely corresponding. The average deviations of Cr_2O_3 and V_2O_3 contents are 0.33 and 0.22 wt%, respectively. This agreement is rated excellent considering the different sampling areas of EPMA and LA-ICP-MS and the expected chemical variation within the sample. The major components of epidote-group minerals contributing to Cr- and V-rich clinozoisite from Outokumpu are $Ca_2Al_3Si_3O_{12}(OH)$ (clinozoisite), $Ca_2Al_2Cr^{3+}Si_3O_{12}(OH)$ (''tawmawite'') and $Ca_2Al_2V^{3+}Si_3O_{12}(OH)$ (mukhinite). The individual site-specific cation concentrations for crystals 1A and 1C slightly deviate (*e.g.*, Ca deficiency) from ideal values (Table 2). This is probably due to low crystallinity of this sample as discussed below.

The specimen from Iratsu, Japan is characterized by high Cr_2O_3 (5.6 wt%), high Fe_2O_3 (8.5 wt%), small amount of SrO (1.7 wt%) and lack of V_2O_3. Fe in Iratsu epidote is only ferric as indicated by ^{57}Fe Mössbauer analysis

Table 2. Representative single spot EPMA analyses and formulae of Cr-rich and Cr-bearing clinozoisites and epidote.

	Outokumpu, Finland					
	1A	1C (Max. Cr content)	1E	2E	Max. V content	Iratsu, Japan
SiO_2	38.55	37.91	38.02	37.78	37.18	36.81
TiO_2	0.11	0.06	0.17	0.14	0.02	0.16
Al_2O_3	28.97	19.92	24.07	23.32	18.02	23.03
Cr_2O_3[a]	5.03	14.01	9.16	9.82	12.68	5.62
Fe_2O_3[a]	0.38	0.11	0.38	0.29	0.27	8.53
V_2O_3[a]	0.96	3.51	1.97	3.16	7.93	–
MnO[a]	0.04	0.00	0.08	0.00	0.04	0.15
MgO	0.18	0.08	0.16	0.17	0.03	0.08
CaO	22.79	22.22	23.42	23.33	22.65	22.00
SrO	–	–	–	–	–	1.70
Na_2O	0.01	0.00	0.00	0.00	0.02	0.06
K_2O	0.02	0.02	0.01	0.01	0.00	0.02
P_2O_5	0.08	0.01	0.05	0.04	0.00	–
La_2O_3	–	–	–	–	–	0.07
Ce_2O_3	–	–	–	–	–	0.11
F^-	0.08	0.14	0.20	0.01	0.00	–
Total	97.20	97.99	97.69	98.07	98.84	98.34
Total cations = 8						
Si	3.01	3.05	3.01	2.99	2.99	2.95
Ti	0.01	0.00	0.01	0.01	0.00	0.01
Al	2.66	1.89	2.24	2.17	1.71	2.17
Cr^{3+}	0.31	0.89	0.57	0.61	0.81	0.36
Fe^{3+}	0.02	0.01	0.02	0.02	0.02	0.51
V^{3+}	0.06	0.23	0.13	0.20	0.51	–
Mn^{2+}	0.00	0.00	0.01	0.00	0.00	0.01
Mg	0.02	0.01	0.02	0.02	0.01	0.01
Ca	1.90	1.92	1.99	1.98	1.95	1.89
Sr	–	–	–	–	–	0.08
Na	0.00	0.00	0.00	0.00	0.00	0.01
K	0.00	0.00	0.00	0.00	0.00	0.00
P	0.01	0.00	0.00	0.00	0.00	–
La	–	–	–	–	–	0.00
Ce	–	–	–	–	–	0.00
Total	8.00	8.00	8.00	8.00	8.00	8.00
Sum of $Cr^{3+} + Fe^{3+} + V^{3+}$	0.39	1.13	0.72	0.83	1.34	0.87

Note: [a] Total Cr, Fe, V and Mn as Cr_2O_3, Fe_2O_3, V_2O_3 and MnO, respectively.

(Nagashima *et al*., 2007). The Cr-bearing epidote is divided into three types: (1) Ca-rich (<3 wt% SrO and REE-free) (2) Sr-rich (3-11 wt% SrO), and (3) REE-rich (3–10 wt% REE_2O_3; mainly Ce, La and Nd). The studied epidote is of type (1). The Cr-bearing epidote has zonal structure characterized by Ca ↔ Sr and Ca + M^{3+} ↔ REE^{3+} + M^{2+} substitutions. The Cr distribution is not related to the zonal structures mentioned above, but the high concentration of Cr generally occurs around or along the vicinity of chromite grains (Nagashima *et al*., 2006).

The Cr-rich clinozoisite (1A, 1C, 1E and 2E) and Cr-bearing epidote (Iratsu) crystals used for electron microprobe analyses (Table 2) and for X-ray single-crystal refinement were identical.

3.1.2. An unidentified sheet-silicate-like Cr-rich mineral in Outokumpu specimens

An unidentified sheet-silicate-like phase is commonly associated with Outokumpu clinozoisite (Fig. 1). The thin nature of the layers characteristic of this sheet-silicate-like phase may be responsible that precise analytical EPMA data are difficult to collect due to overlap with underlying Cr-rich clinozoisite. However, its chemical composition is roughly represented as: 40 wt% SiO_2, 20 wt% Al_2O_3, 6 wt% Cr_2O_3, 1–1.5 wt% FeO, 10–13 wt% CaO, 1 wt% $Na_2O + K_2O$, and < 0.5 wt% V_2O_3, <0.5 wt% MnO and <0.5 wt% MgO (total oxides = *ca.* 81–83 wt%).

3.2. Structural analysis of Cr-rich clinozoisite and epidote

Crystallographic data and refinement parameters are summarized in Table 1. The refined atomic positions and anisotropic displacement parameters are listed in Tables 3 and 4. Interatomic distances and angles are presented in Tables 5 and 6, respectively. Table 7 gives the site-scattering values and cation assignments. Tables 3–6 are freely available online on the GSW website of the journal at http://

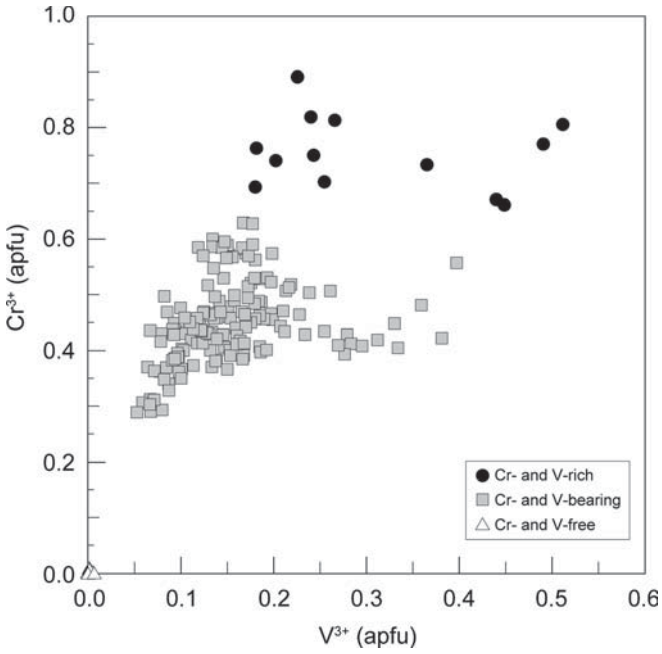

Fig. 2. Variation of Cr and V contents (apfu) of clinozoisite from Outokumpu, Finland. Filled circles represent Cr- and V-rich clinozoisite, gray squares Cr- and V-bearing clinozoisite, and open triangles Cr- and V-free clinozoisite. Notice the gap of compositions between (Cr + V)-bearing and (Cr + V)-free clinozoisite.

geoscienceworld.org/. The crystal structure of Cr-rich clinozoisite is shown in Fig. 3.

Considering the relatively large size of the Outokumpu crystal fragments used for X-ray experiments the diffraction behavior was very poor compared to other clinozoisites and epidotes recently studied in our laboratory. Thus, long X-ray exposure times had to be chosen to obtain a single-crystal diffraction pattern of average reflection intensity within about 5 % accuracy. Furthermore, the X-ray reflections of Finnish Cr-rich clinozoisite appeared as unusual large spherical spots surrounded by a diffuse halo. Corresponding diffraction behavior was only known to us for strongly metamict materials. With increasing heating temperature (up to 750 °C) and annealing time the diffraction behavior only slightly improved but never reached the quality of Cr- and V-free clinozoisite picked adjacent to Cr- and V-rich crystals. In addition, the unit-cell parameters of crystals 1A and 1C crystals measured at room temperature were much larger than expected based on chemical compositions. With increasing annealing temperature, unit-cell parameters decrease. The (Cr + V) contents derived from refined site-occupancies at M1 and M3 (Table 7) were considerably lower than those obtained by chemical analyses (Table 2).

3.3. Samples crystallinity monitored by HRTEM and EBSD

The crystallinity of samples from Outokumpu, Finland was investigated by HRTEM and SEM-EBSD analyses. Both types of analyses indicate that Cr- and V-rich clinozoisite from Outokumpu has low crystallinity. On the other hand, Cr- and V-free and Al-rich counterparts analyzed adjacent to Cr- and V-rich clinozoisite are well crystalline. As shown in Fig. 4, (Cr + V)-free clinozoisites clearly show sharp electron diffraction spots (a) whereas Cr- and V-rich crystals appear almost amorphous in their electron diffraction behavior (b). TEM-EDX measurements on different areas yielded very poor diffraction (up to almost no diffraction) for Cr-rich compositions. Image quality maps of spatial resolution constructed from electron back-scattered diffraction data using various IQ matrices (EBSD by SEM) indicate that Cr- and V-free clinozoisite had higher crystallinity than Cr- and V-rich clinozoisite (Fig. 5). Within large areas intergrown Cr- and V-free clinozoisite and Cr- and

Table 7. Refined site occupancies and number of electrons for the M1, M3 and A2 sites.

Outokumpu, Finland		M1[a]	No. e$^-$	M3[a]	No. e$^-$	A2[b]	No. e$^-$
1A	No treatment	Al0.94(2)M0.06(2)	13.68	Al0.91(2)M0.09(2)	13.94	Ca1.0	20
	500°C, 20 h	Al0.91(1)M0.09(1)	13.98	Al0.87(1)M0.13(1)	14.42	Ca1.0	20
	600°C, 20 h	Al0.89(1)M0.11(1)	14.18	Al0.83(1)M0.17(1)	14.82	Ca1.0	20
	700°C, 20 h	Al0.911(7)M0.089(7)	13.98	Al0.846(8)M0.154(8)	14.69	Ca1.0	20
	750°C, 20 h	Al0.912(7)M0.088(7)	13.96	Al0.858(8)M0.142(8)	14.56	Ca1.0	20
1C	No treatment	Al0.66(2)M0.34(2)	16.73	Al0.64(2)M0.37(2)	17.01	Ca1.0	20
	600°C, 48 h	Al0.65(1)M0.35(1)	16.90	Al0.66(1)M0.34(1)	16.74	Ca1.0	20
	750°C, 48 h	Al0.61(2)M0.39(2)	17.32	Al0.70(2)M0.30(2)	16.30	Ca1.0	20
1E	No treatment	Al0.817(4)M0.183(4)	15.01	Al0.574(4)M0.426(4)	17.69	Ca1.0	20
	700°C, 24 h	Al0.820(4)M0.180(4)	14.98	Al0.592(4)M0.408(4)	17.49	Ca1.0	20
2E	No treatment	Al0.809(6)M0.191(6)	15.10	Al0.582(7)M0.418(7)	17.60	Ca1.0	20
Iratsu, Japan	No treatment	Al0.898(4)Cr0.102(4)	14.12	Al0.451(3)Cr0.039(3)Fe0.51[c]	20.06	Ca0.92Sr0.08	21.44

[a]M at M1 and M3 in Outokumpu samples represents the (Cr + V) content. During the refinement it was treated as Cr.
[b]A2 in Outokumpu samples was fixed as Ca1.0.
[c]Fe population at M3 in Iratsu sample was fixed based on the results of chemical composition and Mössbauer spectrum by Nagashima *et al.* (2007).

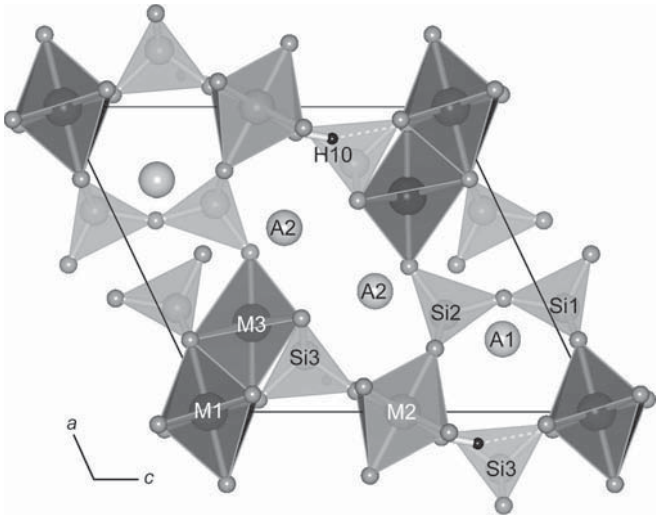

Fig. 3. Crystal structure of Cr-rich clinozoisite projected parallel to [010] using the program VESTA (Momma & Izumi, 2008).

behavior that strongly resembles metamict materials (Fig. 4 and 5). However, adjacent (Cr + V) free clinozoisite produces excellent diffraction patterns. Actually, the electron diffraction behavior of (Cr + V)-rich clinozoisite (Fig. 4) is inferior to the quality of X-ray diffraction, which may be related to the smaller sampling area in electron diffraction covering a lower number of coherent domains.

There is no quantitative relation between (Cr + V) content and diffraction behavior. Very poor X-ray diffraction was found for crystal 1A with 5.03 wt% Cr_2O_3 and also for 1C with 14.01 wt% Cr_2O_3 whereas crystals 1E and 2E with ca. 9.5 wt% Cr_2O_3 (Table 2) produced a fair diffraction pattern. Crystal fragments with varying alphabetic character designation, studied with X-rays, were picked from different source crystals. Thus partial amorphization seems to be variable in (Cr + V)-rich domains of different mother crystals.

The term metamict is reserved for minerals that lose their crystal structure due to radioactive elements. In the

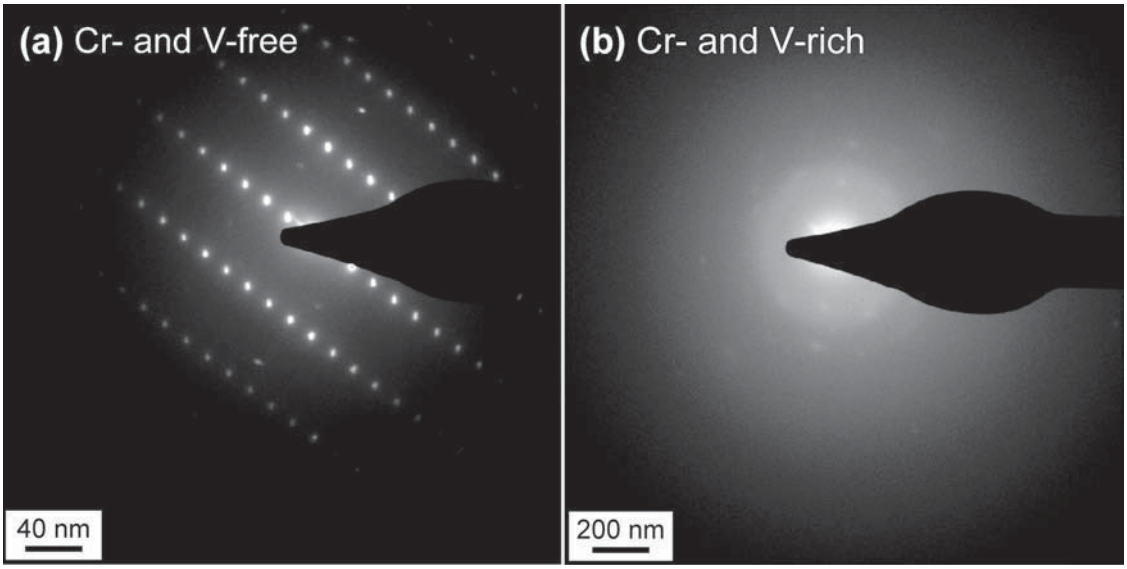

Fig. 4. SAED patterns of Cr- and V-free (a) and Cr and V-rich – almost amorphous – (b) clinozoisite from Outokumpu, Finland.

V-rich clinozoisite show the same orientation as derived from corresponding EBSD behavior.

In addition, the unidentified sheet-silicate-like Cr-rich mineral was also analyzed by EBSD. This phase did not produce any EBSD diffraction patterns, thus its true nature remains unknown.

4. Discussion

4.1. X-ray and electron scattering behavior

As mentioned in the Results section, (Cr + V)-rich clinozoisite from Outokumpu shows a diffraction

original sense metamictization is the destruction of the regular internal structure of a mineral produced by radiations from contained radioactive elements. The metamictization of minerals can be dissipated and the original structure restored by heating them to about 450–900 °C, depending upon the mineral and the rate and time of heating (McGraw-Hill, 1960).

If we accept this latter definition, (Cr + V)-rich clinozoisite cannot be considered metamict because our analyses failed substantiating significant U and Th or even REE commonly accompanying U and Th. In addition, we did not find any U- or Th-bearing mineral in the source rocks. Thus, a radioactivity origin of the poor diffraction behavior can be excluded and we should thus avoid the term metamict.

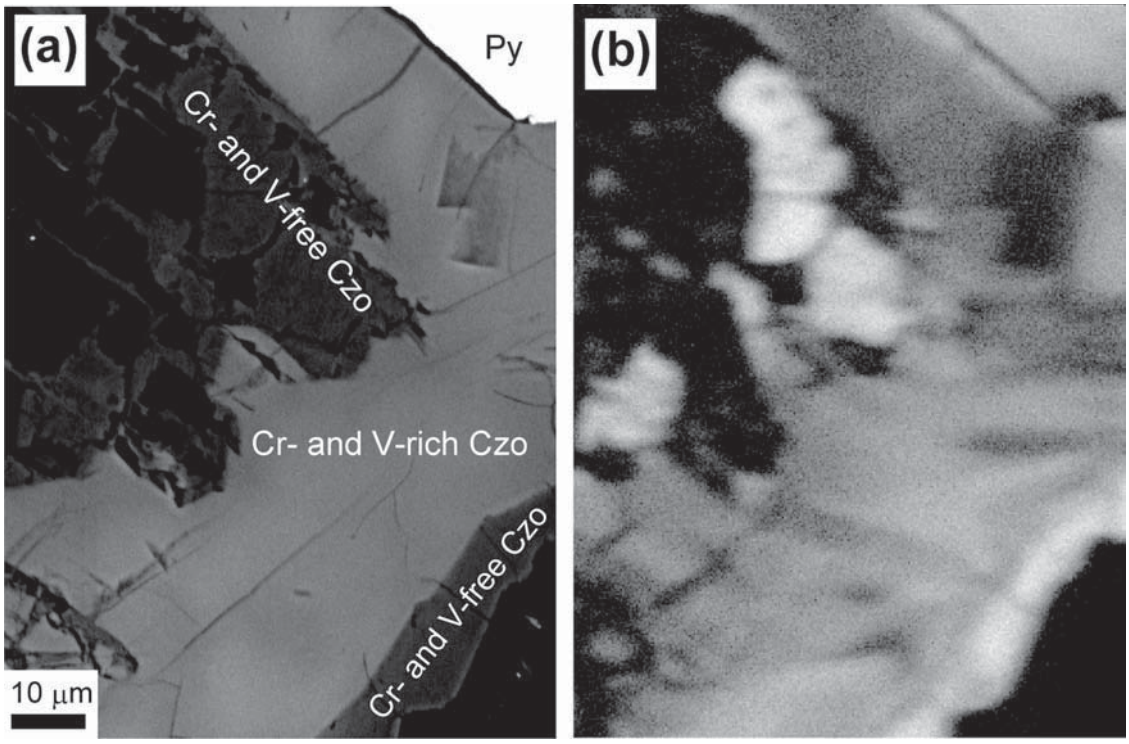

Fig. 5. BSE image (a) and EBSD image quality map (b) of studied specimen. Light contrast indicates good diffraction quality, dark contrast poor diffraction quality.

However, we can imagine other geological or anthropic processes leading to a continuous destruction of the crystal structure or gradual loss of periodicity. Friction, plastic deformation or polishing (Libowitzky, 1994) are among the known mechanisms. Characteristic of zeolites and other framework structures is their pressure and temperature induced amorphization (Greaves, 2001). But at first glance the unusual behavior of (Cr + V)-rich clinozoisite cannot be easily explained by these additional processes leading to poor diffraction behavior.

4.2. Inconsistency between Cr (+V) determined analytically and obtained by structure refinement

The observation that the quality of the diffraction pattern is strongly related (in a qualitative sense) to the (Cr + V) content of clinozoisite indicated that amorphization of clinozoisite is somehow connected with these ions. This is verified by the structure refinements leading to large difference of Cr (+V) contents derived from refined site-occupancies and from microprobe or LA-ICP-MS analyses. *e.g.*, untreated crystal 1C from Outokumpu contains 1.12 (Cr + V) apfu derived from chemical analysis (Table 2) but only 0.70 apfu could be located by structural analysis (Table 7), which is a difference of ca. 37 %. Increasing annealing at 600 and 750°C improved crystallinity and reduced the unit-cell volume by 1.4 % (Table 1) but heat treatment did not lead to higher Cr (+V) occupancies in the structure of clinozoisite. All other analyzed crystals behaved correspondingly. Based on these observations we hypothesize that (1) a Cr-rich epidote-group mineral with composition according to our analytical results (Table 2) was stable at specific metamorphic conditions (*p*, *T*, fluid regime), (2) after retrograde change of these conditions, destruction of the clinozoisite structure was accompanied by exsolution of a Cr-rich amorphous phase. Subsequent heat treatment did not lead to re-accommodation of the exsolved Cr-phase but slightly improved crystallinity of clinozoisite with less (Cr + V) than assumed from the bulk composition.

As an example, even in the simple system Al_2O_3–Cr_2O_3 with isotypic end-members (corundum structure type) there is a strongly pressure dependent solvus (Fujita *et al*., 2007 and references therein). However, as characteristic of sesquioxides, exsolved Cr-poor corundum and Al-rich eskolaite are both crystalline. We speculate that in case of Cr-rich clinozoisite a low-temperature miscibility gap exists. The exsolved Cr-rich phase is amorphous because under retrograde conditions a Cr-rich clinozoisite is not stable and the activation energy is not sufficient to transform the exsolved product into a crystalline assemblage stable under these conditions. This model would also suggest that the exsolution process is governed by kinetics, which could explain the strongly differing partition coefficients and the varying structural damage observed for the crystalline relics.

The inconsistency of Cr content refined from site occupancies (0.22 apfu) and measured by electron-microprobe (0.30 apfu) has also been noted by Nagashima *et al*. (2007). However, they related the observed misfit to heterogeneity

within the crystal. In this study, Cr-rich epidote from Iratsu (Nagashima *et al*., 2007) was measured to confirm the compositional difference. In this new experiment the Cr content derived from structural analysis was 0.14 apfu instead of 0.36 apfu from chemical analysis.

Another confusing aspect is evident for the various refined Me^{3+} (Cr^{3+} and V^{3+}) populations at M3 and M1. There seems to be no consistent partitioning between M1 and M3. For crystal 1A (EPMA: 5.03 wt% Cr_2O_3) the partitioning coefficient ($K_D = (Cr^{3+}/Al)^{M1}/(Cr^{3+}/Al)^{M3}$) is *ca.* 0.65 but *ca.* 1 for 1C (EPMA: 14.01 wt% Cr_2O_3). For the crystals 1E and 2E with best diffraction properties and intermediate composition (EPMA: 9.5 wt% Cr_2O_3) K_D is only *ca.* 0.33. Any interpretation of this behavior is abandoned because the role of minor V^{3+} in the assumed exsolution process and in M3-M1 site preference is unknown.

The inconsistency of chemical composition derived from site scattering (X-ray structure refinement) and measured by EPMA for epidote-group minerals is not new. Bonazzi *et al.* (2009) showed that a truly metamict allanite-group mineral displayed a bulk chemical composition that yielded a strongly non-stoichiometric formula if normalized to 8 cations or 3 Si. In a multi-analytical approach they could show that the results of the structure refinement were correct and that EPMA analyses were biased by the presence of SiO_2 enriched metamict areas. After a corresponding correction for excess SiO_2 the formula became stoichiometric without significant vacancies at any site.

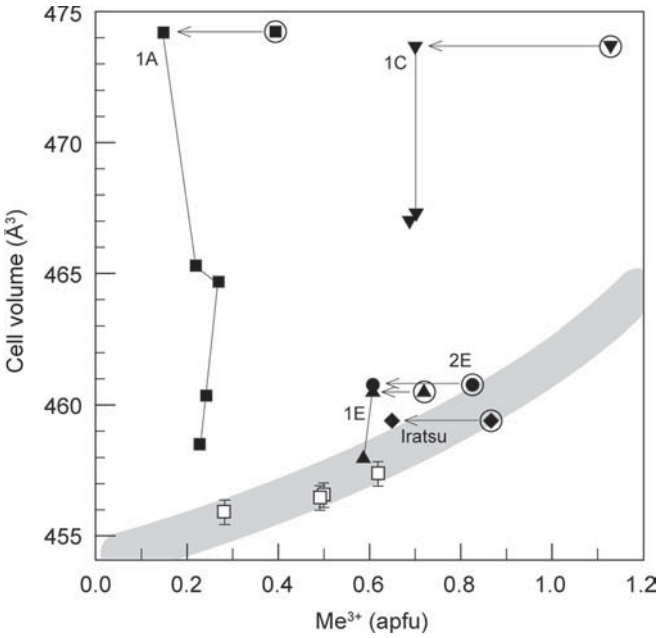

Fig. 6. Variation of cell volume *versus* Me^{3+} ($= Cr^{3+} + Fe^{3+} + V^{3+}$) contents (apfu). Filled symbols represent the results from this study; squares 1A, inverted triangle 1C, triangle 1E, circle 2E and diamond Iratsu. Symbols connected by solid lines towards decreasing volume show the development with increasing annealing temperature. Circled symbols represent the Me^{3+} content determined by microprobe analysis. Open squares represent the data of synthetic Al-Cr^{3+} clinozoisite with 1σ standard deviation (Nagashima *et al*., 2009). The gray ribbon shows the regression curves of Al-Fe^{3+} epidotes summarized by Franz & Liebscher (2004).

4.3. Structural variation of Cr and V-rich clinozoisite

Excessively large unit-cell parameters, which decrease with increasing temperature and annealing duration, are also typically observed in metamict REE-rich epidote-group minerals. The decrease of the unit-cell volume with annealing is caused by re-crystallization (*e.g.,* Bonazzi *et al.*, 2009). A corresponding behavior is also found for our Cr- and V-rich clinozoisite. In particular for those crystals with very poor diffraction behavior, prolonged heating could not readjust the unit-cell volume to the expected range. The expected range was estimated from unit-cell volumes of epidotes with varying Fe^{3+} content (Fig. 6). This procedure seems admissible as high spin Fe^{3+} (0.645 Å) has only a slightly larger ionic radius for octahedral coordination (Shannon, 1976) than Cr^{3+} (0.615 Å) and V^{3+} (0.640 Å), but all three are significantly larger than Al (0.535 Å). Crystal 1E with fair diffraction behavior also displayed a unit-cell volume which upon heating adjusted to the expected range.

A corresponding ''expected range'' can also be defined for mean M3-O and M1-O distances derived from epidote structural data with refined Fe^{3+} occupancy (Fig. 7). As already found for the unit-cell volume behavior upon heating, crystals 1A and 1C show longer M3-O distances than assumed from site-occupancy refinement whereas M3-O distances for crystals 1E, 2E and Iratsu are within the predicted range. Due to lack of reliable reference data, the Me^{3+} population *versus* mean M1-O distance relation is less precisely defined. Nevertheless, M1-O distances of (Cr + V)-rich clinozoisites fit much better to expected and extrapolated values than corresponding M3-O distances.

In our structure refinements of Outokumpu (Cr + V)-rich clinozoisite the strongest difference-Fourier peak comprising 1.0-2.3 electrons (Table 8), not in accordance with epidote-like atomic sites, always appears at a similar position (0.16, 1/4, 0.30). A corresponding peak was observed in untreated and heated allanite-subgroup crystals (Bonazzi *et al*., 2009). The location of this peak is approximately at the barycenter of a tetrahedral cavity defined by O2-O2-O10-O4 atoms (Bonazzi *et al*., 2009; see their Fig. 5). In addition, this ''site'' is along **b** halfway between two orthosilicate Si3 positions. If occupied, this additional site would connect Si3 tetrahedra to a trimer. This peak position also corresponds to that reported as H site in untreated dissakisite-(La) (Lavina *et al*., 2006). Bonazzi *et al*. (2009) concluded that the presence of this ''ghost'' peak could be regarded as a sign of radiation damage, or in our case a consequence of low crystallinity. The ''ghost'' peak was not observed in well crystallized Cr-bearing epidote from Iratsu, for which structure refinement also demonstrated Cr deficit. In our structure refinements of Outokumpu (Cr + V)-rich clinozoisite there is also a second recurring peak (Table 8) of ca. 0.8 electron close to M3, which has no analogue among epidote-like atomic sites.

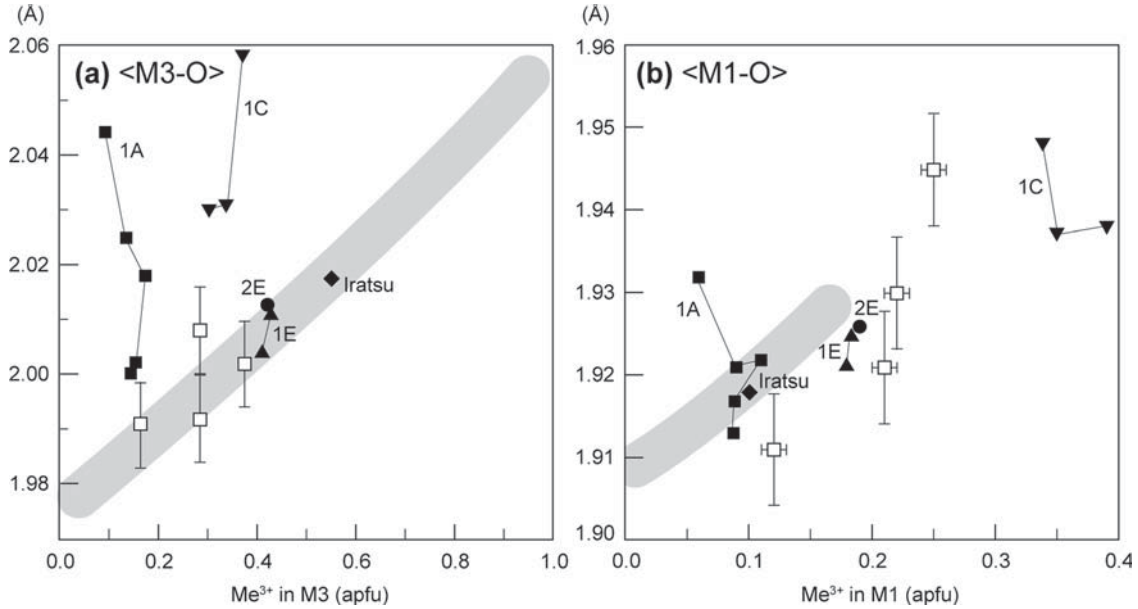

Fig. 7. Variation of <M3-O> (a) and <M1-O> (b) distances *versus* Me^{3+} (= $Cr^{3+} + Fe^{3+} + V^{3+}$) contents (apfu) at each site. The gray ribbon was drawn from the regression curves of Al-Fe^{3+} epidotes summarized by Franz & Liebscher (2004). Symbols as in Fig. 6.

One of the major problems in collecting diffraction data for poorly crystalline materials is scan truncation (point detector) or intensity integration in a too narrow window (area detector). If X-ray reflections are surrounded by a diffuse halo, diffraction spots merge more or less continuously with the background. This type of truncation particularly decreases the intensity of strong reflections. Being aware of this problem, we have performed intensity integration tests with strongly reduced and augmented window size but the ''ghost'' peaks persisted. Another explanation could be stacking faults along the **b**-axis. Thus the strongest ''ghost'' peak approximately coincides with Si3 displaced by 1/2 along **b**. However, such stacking faults should also be confirmed by other sites with even stronger scattering power such as Ca at A1 and A2. This is not observed. Most probably, these ''ghost'' peaks are related to inadequate handling of diffuse scattering and treating such phenomena as ''relics'' of Bragg reflections.

5. Conclusion

Evidence shown in this paper and in the studies by Treloar (1987a, b) suggests that a mineral of $CaAl_2Cr^{3+}Si_3O_{12}(OH)$ composition once existed in the quartzites of Outokumpu. With a slight preference of Cr for M3, the above analytically determined (EPMA) composition would at first glance already be sufficient to revive the mineral name ''tawmawite''. However, the original composition could not be re-established by heat treatment. This implies that for the crystals investigated by us the physical properties of $CaAl_2Cr^{3+}Si_3O_{12}(OH)$ cannot be determined, which alone disqualifies revival of the name ''tawmawite'' for (Cr + V)-rich clinozoisite from Outokumpu, Finland. This conclusion is in full agreement with the remarks on nomenclature by Bonazzi *et al.* (2009) suggesting that their allanite-group mineral theoretically deserves a new root-name but strong amorphization and the existence of inclusions inhibit determination of physical properties required for acceptance of a new mineral species.

The superb optical quality with well defined anisotropy of Outokumpu (Cr + V)-rich clinozoisite is not in contrast to its very poor diffraction behavior. Anisotropic optical properties are due to orientation-dependent electronic polarizabilities of valence electrons under the influence of the electric field tensor (*e.g.*, Armbruster, 1985). The electric field tensor reflects the structure-specific atomic arrangement. Thus, periodicity required for diffraction is not a prerequisite for optical anisotropy. Even a fragmented structure still preserves optical anisotropy if the structural motif maintains corresponding alignment.

Our results indicate that (Cr + V)-rich clinozoisite with poor diffraction behavior has a strongly disturbed lattice periodicity. Furthermore, the high (Cr + V) content of the crystals determined by EPMA and LA-ICP-MS could not be confirmed by site-occupancy crystal-structure refinements, not even after prolonged annealing. Thus, excess (Cr + V) is not part of the clinozoisite structure. The observations suggest that Cr-rich nano-domains exsolved from originally (Cr + V)-rich clinozoisite on the retrograde path, interrupting lattice periodicity. Subsequent experimental annealing of the composite material cured to some degree the faulty structure of the clinozoisite, but the exsolved Cr-rich phase could not be resorbed.

We do not believe that the ubiquitous, probably exsolved, unidentified Cr-rich sheet-silicate-like phase observed within clinozoisite has a direct bearing on the poor crystallinity and site occupancy problems of (Cr + V)-rich clinozoisite. The Al/Cr ratio of the unidentified silicate is always close to adjacent clinozoisite and not Cr-enriched.

Table 8. The strongest and second strongest positive difference-Fourier peaks of Cr-rich clinozoisite.[a]

		Strongest peak					Second strongest peak				
Outokumpu, Finland		*x*	*y*	*z*	No. e$^-$	Distances (Å) from the nearest atoms	*x*	*y*	*z*	No. e$^-$	Distances (Å) from the nearest atoms
1A	No treatment	0.164	1/4	0.309	2.33	1.65 from O4	0.384	1/4	0.215	1.49	0.86 from M3
	500°C, 20 h	0.160	1/4	0.304	1.79	0.78 from H10, 1.59 from O4	0.375	1/4	0.204	1.00	0.84 from M3
	600°C, 20 h	0.165	1/4	0.305	1.54	0.83 from H10, 1.60 from O4	0.377	1/4	0.207	0.75	0.85 from M3
	700°C, 20 h	0.167	1/4	0.298	1.27	1.01 from H10, 1.54 from O4	0.383	1/4	0.222	0.54	0.84 from M3
	750°C, 20 h	0.168	1/4	0.299	1.28	1.07 from H10, 1.55 from O4					
1C	No treatment	0.168	1/4	0.304	2.10	0.86 from H10, 1.59 from O4	0.376	1/4	0.184	1.25	0.95 from M3
	600°C, 48 h	0.163	1/4	0.298	2.06	1.19 from H10, 1.52 from O4	0.383	1/4	0.206	0.89	0.88 from M3
	750°C, 48 h	0.178	1/4	0.306	1.83	0.90 from H10, 1.60 from M3	0.536	0.94	0.401	0.78	1.21 from A2
1E	No treatment	0.156	1/4	0.303	1.85	0.88 from H10, 1.57 from O4	0.697	3/4	0.103	0.92	0.58 from A1
	700°C, 24 h	0.159	1/4	0.304	0.93	0.99 from H10, 1.58 from O4					
2E	No treatment	0.158	1/4	0.304	1.05	0.83 from H10, 1.58 from O4					

Note: [a]The peaks more than 0.5 e Å^{-3} are listed. The Cr-rich epidote from Iratsu, Japan has no positive difference Fourier peaks more than 0.5 e Å^{-3}.

Acknowledgements: We thank Dr. Sergey Krivovichev, chief editor, Dr. Marco Pasero, associate editor, Dr. Peter Bačik, and Dr. Paola Bonazzi for their constructive comments on this manuscript. We also thank Mr. Vladimir Malogajski for his assistance with photomicrographs and structural measurements. Mineral samples for our studies were kindly given by Mr. Ilkka Mikkola, Mr. Pekka Paananen and Dr. Martti Lehtinen from the Mineral Cabinet of the Finnish Museum of Natural History, University of Helsinki. Part of this study was supported by Grant-in-Aid for Research Activity Start-up (No. 22840029) promoted by The Ministry of Education, Culture, Sports, Science and Technology-Japan (MEXT).

References

Ashley, P.M. & Martyn, J.E. (1987): Chromium-bearing minerals from a metamorphosed hydrothermal alteration zone in the Archean of Western Australia. *N. Jb. Mineral. Abh.*, **157**, 81–111.

Armbruster, T. (1985): Kristalloptik transparenter Minerale in sichtbarem Licht. *Fortschritte der Mineralogie*, **63**, 91–109.

Armbruster, T., Bonazzi, P., Akasaka, M., Bermanec, V., Chopin, C., Heuss-Assbichler, S., Liebscher, A., Menchetti, S., Pan, Y., Pasero, M. (2006): Recommended nomenclature of epidote-group minerals. *Eur. J. Mineral.*, **18**, 551–567.

Bačík, P. & Uher, P. (2010): Dissakisite-(La), mukhnite, and clinozoisite: (V,Cr,REE)-rich members of the epidote group in amphibole – pyrite – pyrrhotite metabasic rocks from Pezinok, Rybnicek, western Carpathians, Slovakia. *Can. Mineral.*, 48, 523–536.

Bastin, G.F., van Loo, F.J.J., Heijlingers, H.J.M. (1984): Evaluation of the use of Gaussian $\phi(\rho z)$ curves in quantitative electron probe microanalysis: a new optimization. *X-ray Spectrom.*, **13**, 91–97.

Bastin, G.F., Heijlingers, H.J.M., van Loo, F.J.J. (1986): A further improvement in the Gaussian $\phi(\rho z)$ approach for matrix correction in quantitative electron probe microanalysis. *Scanning*, **8**, 45–67.

Baur, H. (1974): The geometry of polyhedral distortions. Predictive relationships for the phosphate group. *Acta Crystallogr.*, **B30**, 1195–1215.

Bonazzi, P., Holstam, D., Bindi, L., Nysten, P., Capitani, GC. (2009): Multi-analytical approach to solve the puzzle of an allanite-subgroup mineral from Kesebol, Västra Götaland, Sweden. *Am. Mineral.*, **94**, 121–134.

Bleeck, A.W.G. (1907): Die Jadeitlagerstätten in Upper Burma. *Z. praktische Geol.*, **1907**, 341–365.

Bruker (1999): SMART and SAINT-Plus. Versions 6.01. Bruker AXS Inc., Madison, WI.

Burns, R.G. & Strens, R.G.J. (1967): Structural interpretation of polarized absorption spectra of the Al-Fe-Mn-Cr epidotes. *Mineral. Mag.*, **36**, 204–226.

Devaraju, T.C., Raith, M.M., Spiering, B. (1999): Mineralogy of the Archean barite deposit of Ghattihosahalli, Karnataka India. *Can. Mineral.* **37**, 603–617.

Dollase, W.A. (1968): Refinement and comparison of the structures of zoisite and clinozoisite. *Am. Mineral.*, **53**, 1882–1898.

Enraf-Nonius (1983): Structure determination package (SDP) (computer program), Enraf Nonius, Delft, The Netherlands.

Eskola, P. (1933): On the chrome minerals of Outokumpu. *Bulletin de la Commission géologique de Finlande*, **103**, 26–44.

Franks, F., Ed. (1973): Water: a comprehensive treatise, **2**, Plenum, New York.

Franz, G. & Liebscher, A. (2004): Physical and chemical properties of the epidote minerals – An introduction -; in Epidotes, Eds. Liebscher, A. and Franz, G.; Reviews in Mineralogy & Geochemistry, Vol. 56; Mineralogical Society of America, Geochemical Society, 1–82.

Fujita, M., Inukai, K., Sakida, S., Nanba, T., Ommyoji, J., Yamaguchi, A., Miura, Y. (2007): Sintering of Al_2O_3-Cr_2O_3 powder prepared by sol-gel process. *J. Soc. Mater. Sci. Jpn*., **56**, 526–530.

Grapes, R.H. (1981): Chromian epidote and zoisite in kyanite amphibolites, Southern Alps, New Zealand. *Am. Mineral*., **66**, 974–975.

Greaves, G.N. (2001): Compressibility, pressure induced amorphisation and thermal collapse of zeolites. *in* ''Frontiers of High Pressure Research II, Application of High Pressure to Low Dimensional Novel Electronic Materials'', Nato Science Series, Hochheimer, et al., eds., Kluwer Academic Publishers, Dordrecht, The Netherlands, 53–71.

Ito, T., Morimoto, N. & Sadanaga, R. (1954): On the structure of epidote. *Acta Crystallogr*., **7**, 53–59.

Koistinen, T.J. (1981): Structural evolution of an early Proterozoic stratabound Cu-Co-Zn deposit, Outokumpu, Finland. *Trans. R. Soc. Edinburgh Earth Sci.*, **72**, 115–158.

Lavina, B., Carbonin S., Russo, U., Tumiati, S. (2006): The crystal structure of dissakisite-(La) and structural variations after annealing of radiation damage. *Am. Mineral*., **91**,104–110.

Libowitzky, E. (1994): Anisotropic pyrite: a polishing effect. *Phys. Chem. Minerals*, **21**, 97–103.

McGraw-Hill Encyclopedia of Science and Technology (1960): McGraw-Hill Book Company Inc., New York, **6**, 129.

Momma, K. & Izumi, F. (2008): VESTA: a three-dimensional visualization system for electronic and structural analysis. *J. Appl. Crystallogr*., **41**, 653–658.

Nagashima, M., Akasaka, M., Sakurai, T. (2006): Chromian epidote in omphacite rocks from the Sambagawa metamorphic belt, central Shikoku, Japan. *J. Mineral. Petrol. Sci*., **101**, 157–169.

Nagashima, M., Akasaka, M., Kyono, A., Makino, K., Ikeda, K. (2007): Distribution of chromium among the octahedral sites in chromian epidote from Iratsu, central Shikoku, Japan. *J. Mineral. Petrol. Sci*., **102**, 240–254.

Nagashima, M., Geiger, C.A., Akasaka,M. (2009): A crystal-chemical investigation of clinozoisite synthesized along the join $Ca_2Al_3Si_3O_{12}(OH)$-$Ca_2Al_2CrSi_3O_{12}(OH)$. *Am. Mineral*., **94**, 1351–1360.

Packwood, R.H. & Brown, J.D. (1981): A Gaussian expression to describe $\phi(\rho z)$ curves for quantitative electron probe microanalysis. *X-ray Spectrometry*, **10**, 138–146.

Robinson, K., Gibbs, G.V., Ribbe, P.H. (1971): Quadratic elongation: a quantitative measure of distortion in coordination polyhedra. *Science*, **172**, 567–570.

Sánchez-Vizcaíno, V.L., Franz, G., Gómez-Pugnaire, M.T. (1995): The behavior of Cr during metamorphism of carbonate rocks from the Nevado-Filabride complex, Betic Cordilleras, Spain. *Can. Mineral*., **33**, 85–104.

Shannon, R.D. (1976): Revised effective ionic radii and systematic studies of interatomic distances in halides and chalcogenides. *Acta Crystallogr*., **A32**, 751–767.

Sheldrick, G.M. (1996): *SADABS*. University of Göttingen, Germany.

Sheldrick, G.M. (2008): A short history of SHELX. *Acta Crystallogr*., **A64**, 112–122.

Treloar, P. (1987a): Chromian muscovites and epidotes from Outokumpu, Finland. *Mineral. Mag*., **51**, 593–599.

Treloar, P. (1987b): The Cr-minerals of Outokumpu – their chemistry and significance. *J. Petrol*., **28**, 867–886.

Treloar, P. & Charnley, N.R. (1987): Chromian allanite from Outokumpu, Finland. *Can. Mineral*., **25**, 413–418.

Treloar, P. J., Koistinen, T. J., Bowes, D. R. (1981): Metamorphic development of cordierite-orthoamphibole rocks and mica schists in the vicinity of the Outokumpu ore-deposit. *Trans. R. Soc. Edinburgh Earth Sci*., **72**, 201–215.

Uher, P., Kováčik, M., Kubiš, M., Shtukenberg, A., Ozdín, D. (2008): Metamorphic vanadian-chromian silicate mineralization in carbon-rich amphibole schists from the Malé Karpaty Mountains, Western Carpathians, Slovakia. *Am. Mineral.*, **93**, 63–73.

von Knorring, O., Condiffe, E. Tong, Y.L. (1986): Some mineralogical and geochemical aspects of chromian-bearing skarn minerals from northern Karelia. *Bull. Geol. Surv. Finland*, **58**, 277–292.